Sensors and Actuators Reports 3 (2021) 100034

Contents lists available at ScienceDirect

Sensors and Actuators Reports

journal homepage: www.elsevier.com/locate/snr

Novel analysis of a micropillar coupled acoustic wave sensor

Siqi Ji [a,c], Hamed Esmaeilzadeh [a], Junwei Su [a], Sheree Pagsuyoin [b], Hongwei Sun [a,c,*]

[a] Department of Mechanical Engineering, University of Massachusetts Lowell, Lowell, MA, United States
[b] Department of Civil and Environmental Engineering, University of Massachusetts Lowell, Lowell, MA, United States
[c] Department of Mechanical and Industrial Engineering, Northeastern University, Boston, MA, United States

ARTICLE INFO

Keywords:
Quartz crystal microbalance
Acoustic wave sensor
Micropillars
Q-factor

ABSTRACT

Acoustic wave sensors are being developed for many emerging applications such as in semiconductor fabrication, biological diagnostics and polymer characterization. Traditional acoustic wave sensing devices such as quartz crystal microbalance (QCM) rely on polymer thin films coated on quartz plates to detect chemical and biological agents. It has been found that significant sensitivity enhancement of QCM devices can be achieved by simply attaching a polymer micropillar film onto the QCM substrate (QCM-P) to enable a unique coupled resonance between the micropillars and quartz substrate. In the present work, an equivalent circuit model integrating mechanical vibration of micropillars and electrical load impedance of piezoelectric substrate was developed to predict the frequency shift and Q-factor of the QCM-P devices when operating in air and liquid environments. In the model, the vibration of micropillars was solved simultaneously with the liquid loading on the pillar surface. The resultant hydraulic force was integrated into the circuit model to predict the load impedance on the sensor surface. The developed model was validated by experimental results for QCM-P devices operating in air and water with different micropillar heights. It will serve as a powerful tool to predict the performance of the QCM-P devices for different applications.

1. Introduction

Quartz crystal microbalance (QCM) devices, oscillating in thickness shear mode (TSM), is one of the most commonly used mass sensors for a wide range of chemical and biological applications due to its simple, cost-effective, and high-resolution sensing advantages [1]. QCM sensors operating at 10 MHz are capable of detecting a mass variation of less than 10 ng/cm^2 on its surface [2–6]. Traditional QCMs are made on an AT-cut quartz crystal plate with both sides coated with a layer of chromium (adhesion layer) followed by a gold film as the electrodes [7,8]. When an alternating voltage is applied to the two electrodes, a transverse shear wave forms in the substrate because of its crystal orientation and piezoelectric properties. The resonance frequency and bandwidth of the shear wave generated in the substrate change in response to the polymer structure, mass loading, liquid viscosity and density, chemical interaction or cells binding strength occurring on the surface of the substrate [9].

Label-free biomolecular interaction analysis (BIA) detection is an enabling instrument in probing interactions between biomolecules which is being widely used in pharmaceutical discovery and development, immunological and biochemical research, and food analysis. Due to its high-level limit of detection (LOD) (~0.1 ng/cm^2), surface plasmon resonance (SPR) is currently the dominating technology for BIA adopted by biopharmaceutical companies for drug discovery and development [10]. However, SPR systems normally require well-trained personnel to operate and are expensive (up to $750k) [11]. Traditional quartz crystal microbalance (QCM) based systems have relatively low LODs (~10 ng/cm^2) which makes these systems less attractive for BIA applications [12]. Recently, we discovered a new technology which can significantly improve the sensitivity of the QCM sensors by attaching micro-sized pillar arrays made of Polymethyl methacrylate (PMMA) onto the electrodes of QCM (QCM-P) to form a coupled two-degree-of-freedom system [13]. Preliminary studies showed that the unique resonance between micropillars and QCM substrate (as shown in Fig. 1 [14]) can improve surface mass sensitivity by eightfold in bovine serum albumin (BSA) detections [15].

In the two-degree-of-freedom system analysis for Fig. 1, the QCM substrate is treated as an equivalent mass [16–18] and a spring with force constant (k) and PMMA micropillar as the other set of mass (M) and spring (K). As a result, the relationship between the displacements

* Corresponding author at: Northeastern University, Mechanical and Industrial Engineering, United States.
E-mail address: ho.sun@northeastern.edu (H. Sun).

https://doi.org/10.1016/j.snr.2021.100034
Received 13 December 2020; Revised 22 February 2021; Accepted 3 March 2021
Available online 9 March 2021

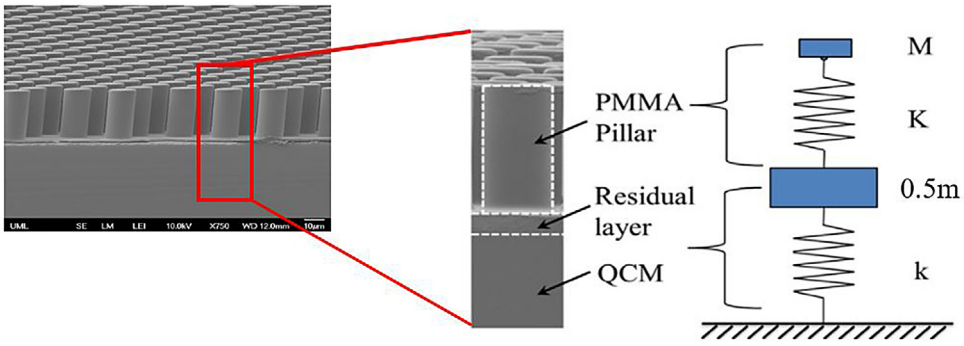

Fig. 1. Two-degree-of-freedom equivalent model for QCM-P sensor [14] (inset: SEM image of micropillars (diameter:12.5 μm, height: 24 μm, and spacing: 33 μm) coated QCM substrate).

(x_1 and x_2) of the QCM and micropillar can be established based on Newton's second law as [15]:

$$\begin{bmatrix} 0.5m & 0 \\ 0 & M \end{bmatrix} \begin{pmatrix} \ddot{x}_1 \\ \ddot{x}_2 \end{pmatrix} + \begin{bmatrix} k+K & -K \\ -K & K \end{bmatrix} \begin{pmatrix} x_1 \\ x_2 \end{pmatrix} = \begin{pmatrix} 0 \\ 0 \end{pmatrix} \tag{1}$$

Solving for the resonance frequency (f) of the coupled system gives

$$f = \frac{1}{2\pi} \sqrt{\frac{1}{2}\left(\frac{k}{m/2} + \frac{K}{m/2} + \frac{K}{M}\right) \pm \frac{1}{2}\left[\left(\frac{k}{m/2} + \frac{K}{m/2} + \frac{K}{M}\right)^2 - 4\frac{k}{m/2}\frac{K}{M}\right]^{\frac{1}{2}}} \tag{2}$$

Experimental studies have shown that the Eq. (2) is able to successfully predict the frequency response of the system [15]. However, the mass-spring system model was not able to identify the energy dissipation or Q-factor during the sensor operation [19–21]. Depending on different geometries of the micropillars or surrounding fluids such as either liquid or air, the Q-factor of QCM-P could vary from 10^2 to 10^5 or even lower when the pillar height approach critical height [13,22] which usually falls below the detection limit (~200) of common frequency counters. In addition, it is questionable that the hydraulic force was simply treated as an added mass to the micropillars in the model [19–21]. There is a need to establish a comprehensive theoretical model to evaluate the new sensor performance in terms of the frequency shift and Q-factor responses and obtain a fundamental understanding of the working principle of QCM-P sensors operating in air and liquid for further performance improvement.

2. Experimental methods

Experimental study was conducted to validate the models developed for QCM-P sensors operating in air and water. PMMA micropillars with circular cross section and diameter of 5 μm and heights from 8 μm, 8.48 μm, 8.71 μm, 9.16 μm, 9.40 μm, 10.85 μm, 13 μm to 14.5 μm, and center-to-center spacing of 16μm were fabricated on the AT-cut quartz surface (see inset of Fig. 1) using nanoimprint method which has been described in previous study [13]. Fig. 2 illustrates the typical conductance curve of micropillar with height of 8 μm in air and in water. For each micropillar height, the conductance vs. frequency curve $\left(Re(1/Z) \text{ vs. } f\right)$ was generated by a network analyzer (HP 8573D, Hewlett-Packard). Both frequency shift and Q-factor are extracted from the conductance curves and compared with the model developed in the next section.

3. Theoretical models

3.1. Equivalent circuit model development of QCM-P device

The Mason circuit model, Butterworth-Van Dyke (BVD) and Krimholtz-Leedom-Matthaei (KLM) models are commonly used four-element or three-port (six terminals) equivalent circuit models for modeling the performance of QCM resonators [23–29]. The key function of these models is to find the load impedance (Z_L) as a function of frequency shift (Δf) based on the equivalent circuits of QCM. Fig. 3 depicts the schematic of the elements and load impedance in the KLM equivalent circuit model [29].

In the KLM model, a mechanical transmission line represents the wave propagation in the piezoelectric resonator with thickness d. Z_1 and Z_2 represent the load impedances acting on the bottom and top surfaces of the resonator. The impedance of crystal itself is divided into two Z_0 representing the quartz characteristic impedance. The $v_{F,B}^{\pm}$ terms represent particle velocities inside of the resonator with different traveling waves propagating directions. The piezoelectric coupling is represented by a transformer with frequency dependent transformer ratio of ϕ. The transformer is connected through the electrostatic capacitance C_0 and a reactance X to the electrical terminals of the resonator. V_3 and I_3 are the applied voltage and current at the electrical terminals which produce the resulting acoustic forces F and particle velocities U at the resonator surfaces [28].

For AT-cut QCM-P sensor, only the top surface is attached to a micropillar layer, therefore, we set $Z_1 = 0$ and $Z_2 = Z_L$. The total acoustic impedance (Z_a) of the circuit is considered as the sum of two parallel impedances on the left and right sides of the acoustic transmission line: Z_{L1} and Z_{L2}, respectively. The three impedances, Z_a, Z_{L1} and Z_{L2}, can be calculated as

$$Z_{L1} = Z_0 \frac{Z_1 + jZ_0 tan\frac{\alpha}{2}}{Z_0 + jZ_1 tan\frac{\alpha}{2}} = jZ_0 tan\frac{\alpha}{2} \tag{3}$$

$$Z_{L2} = Z_0 \frac{Z_2 + jZ_0 tan\frac{\alpha}{2}}{Z_0 + jZ_2 tan\frac{\alpha}{2}} = Z_0 \frac{Z_L + jZ_0 tan\frac{\alpha}{2}}{Z_0 + jZ_L tan\frac{\alpha}{2}} \tag{4}$$

$$Z_a = \frac{Z_{L1}Z_{L2}}{Z_{L1} + Z_{L2}} = Z_0 \frac{Z_L + jZ_0 tan\frac{\alpha}{2}}{2Z_0 + jZ_L\left(tan\frac{\alpha}{2} - \frac{1}{tan\frac{\alpha}{2}}\right)} = \frac{Z_L + jZ_0 tan\frac{\alpha}{2}}{2\left(1 - j\frac{Z_L}{Z_0} cot\alpha\right)} \tag{5}$$

where α is the acoustic phase shift of the QCM-P sensor. As a result, the total impedance (Z) of the KLM model can be calculated as

$$Z = \frac{1}{j\omega C_0} + jX + \frac{1}{\phi^2} Z_a \tag{6}$$

where ω is the operating angular frequency, and $\frac{1}{\phi^2}$ and X in KLM model are known as

$$\frac{1}{\phi^2} = \frac{1}{\omega C_0} \frac{4K^2}{\alpha} \frac{1}{Z_0} sin^2 \frac{\alpha}{2} \tag{7}$$

$$X = \frac{1}{\omega C_0} \frac{K^2}{\alpha} sin\alpha \tag{8}$$

where K is the electromechanical coupling factor and C_0 is the static capacitance arising from gold electrodes located on opposite sides of the QCM sensor. C_0 is calculated to be 4.890 pF [28] and K is 8.8% for AT-cut quartz crystal plate [28].

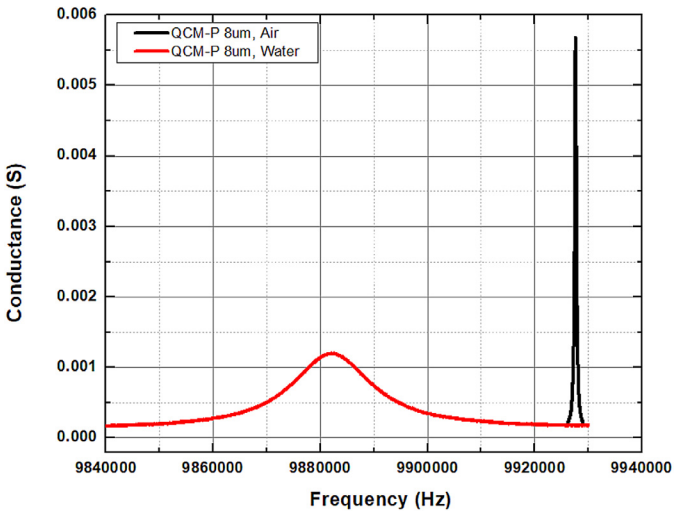

Fig. 2. The conductance curve of QCM-P with pillar height of 8μm operating in air and water.

Substituting Eqs. (7) and (8) into (6), we can obtain the total impedance (Z) of the KLM model as [28,30]

$$Z = \frac{1}{j\omega C_0}\left(1 - \frac{K^2}{\alpha}\frac{2tan\frac{\alpha}{2} - j\frac{Z_L}{Z_0}}{1 - j\frac{Z_L}{Z_0}cot\alpha}\right) \tag{9}$$

where Z_L represents the load impedance induced by the micropillar layer attached on the quartz surface.

3.2. Load impedance of micropillars operating in air

To evaluate the load impendence of micropillar operating in air, $Z_{L,air}$, we applies the Newton's second Law to the differential element of the micropillar of thickness, dz [31] (see Fig. 4), and obtain

$$\kappa AG\frac{\partial^2 u}{\partial z^2}dz = (\rho A dz)\frac{\partial^2 u}{\partial t^2} \tag{10}$$

where $u(z)$ is displacement of the micropillar in the z direction which is parallel to the pillar height direction, κ is Timoshenko shear coefficient of the micropillar, A is cross sectional area of the micropillar, G is complex shear modulus of the micropillar material ($G = G' + jG''$), G' and G'' is the real and imaginary parts of the shear modulus of micropillars, and ρ is the density of the micropillar material. Assuming the micropillar displacement takes a periodic form as

$$u = u(z)\exp(i\omega t) \tag{11}$$

Substituting Eq. (11) into Eq. (10) yields

$$\frac{\partial^2 \boldsymbol{u}}{\partial z^2} + \lambda^2 \boldsymbol{u} = 0 \tag{12}$$

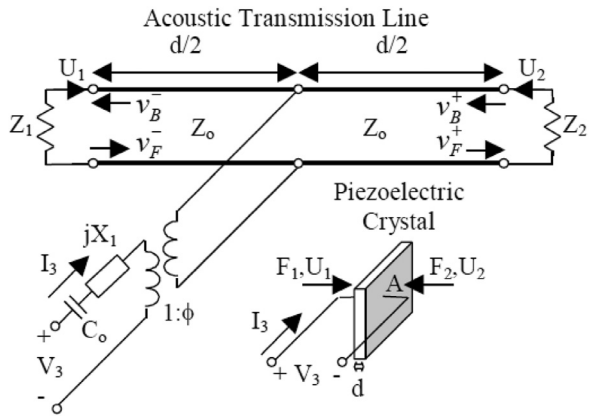

Fig. 3. KLM equivalent circuit of the piezoelectric resonator [29].

where

$$\lambda = \omega\sqrt{\frac{\rho}{\kappa G}} \tag{13}$$

The top surface of micropillar is free of constraint and the boundary conditions of a micropillar is given by

$$\kappa AG\frac{\partial \boldsymbol{u}}{\partial z}|_{z=H} = 0 \tag{14}$$

The base of the micropillar is vibrating with quartz plate, therefore,

$$\boldsymbol{u}|_{z=0} = \boldsymbol{u}_0 \tag{15}$$

where $\boldsymbol{u}_0$ is the displacement of top surface of the quartz plate.

Solving Eq. (12) for the displacement of a micropillar with the two boundary conditions (Eqs. (14) and (15)) gives

$$\boldsymbol{u}(z) = \frac{\boldsymbol{u}_0 cos[\lambda(z - \boldsymbol{H})]}{cos(\lambda \boldsymbol{H})} \tag{16}$$

As a result, the load impedance $\boldsymbol{Z}_{L,air}$ on the surface of the quartz plate can be calculated as [31]

$$\boldsymbol{Z}_{L,air} = -\frac{\hat{\tau}_0}{v_0} = -\frac{\boldsymbol{N}\kappa \boldsymbol{AG}\frac{\partial \boldsymbol{u}}{\partial z}|_{z=0}}{j\omega \boldsymbol{u}_0} = -\frac{\boldsymbol{N}\kappa \boldsymbol{AG}\lambda tan(\lambda \boldsymbol{H})}{j\omega} \tag{17}$$

where $\hat{\tau}_0$ and v_0 are shear stress and velocity of QCM's top surface, respectively. $\boldsymbol{N}$ is the number of micropillars per meter square (m^2) of QCM surface and $\boldsymbol{H}$ is the height of micropillar.

In addition, a thin residual layer (~2μm) is generated between micropillars and QCM surface during the nanoimprinting process. The load impedance induced by the residual layer with thickness of $\boldsymbol{h}$ is added to the load impedance of micropillar as [32,33]

$$\boldsymbol{Z}_{L,air} = -\frac{\boldsymbol{N}\kappa \boldsymbol{AG}\lambda tan(\lambda \boldsymbol{H})}{j\omega} + j\omega \boldsymbol{\rho h} \tag{18}$$

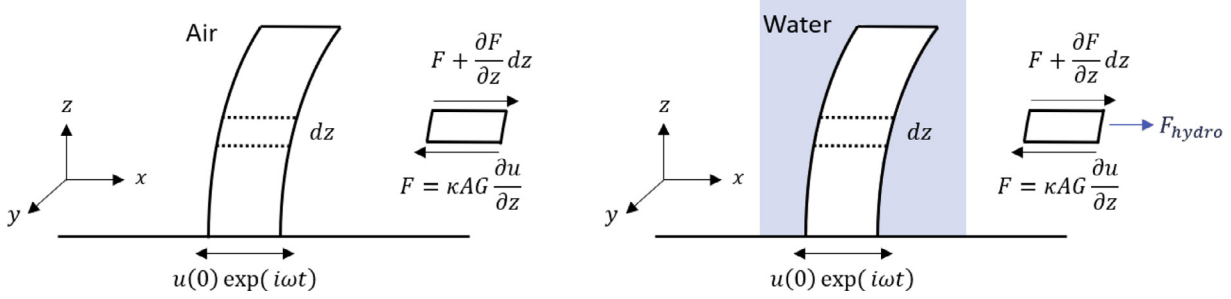

Fig. 4. Force analysis of a differential element of micropillar operating in air and water.

3.3. Load impedance of micropillars operating in liquid

The load impendence of a micropillar operating in water, $Z_{L,liquid}$ can be obtained by adding the hydrodynamic loading F_{hydro} to the LHS of the Eq. (10) due to the interaction between micropillar and the fluid surrounding the micropillar [20] (see Fig. 4). Therefore,

$$\kappa AG\frac{\partial^2 u}{\partial z^2}dz + F_{hydro} = (\rho A dz)\frac{\partial^2 u}{\partial t^2} \tag{19}$$

The hydrodynamic loading F_{hydro} is given by

$$F_{hydro} = \frac{\pi}{4}\rho_l \omega^2 d^2 \Gamma(\omega) u(z) \tag{20}$$

where

$$\Gamma(\omega) = 1 + \frac{4jK_1\left(-j\sqrt{jRe}\right)}{\sqrt{jRe}K_0\left(-j\sqrt{jRe}\right)} \tag{21}$$

$\Gamma(\omega)$ is a well-known hydrodynamic functions of beams with circular cross section operating in liquid [20], where Re is the Reynolds number for flow around micropillars and K_0 and K_1 are modified Bessel functions of the third kind.

As analytical solution of Eqs. (19)–(21) is challenging, the displacement of micropillar $u(z)$ was solved in MATLAB. Young's modulus of PMMA pillar (~5 GPa) was based on the measurement by nanoindentation for microscale sample [34]. The Euler Bernoulli equation [35] is used to describe the deflection of beam in water, $W(z)$ as

$$EI\frac{\partial^4 W(z)}{\partial z^4} + \rho_p A\frac{\partial^2 W(z)}{\partial t^2} = F_{hydro}(z) \tag{22}$$

The micropillar displacement, $u(z)$ can be written as the combination of the pillar displacement at the base u_0 and beam deflection $W(z)$

$$u(z) = u_0 + W(z) \tag{23}$$

Applying modal analysis of beam deflection $W(z)$ [36] gives

$$W(z) = \sum_{n=1}^{100} D_n W_n(z) \tag{24}$$

where $W_n(z)$ is the modal function given by

$$W_n(z) = \lambda_n[cos(\alpha_n z) - ch(\alpha_n z)] + sin(\alpha_n z) - sh(\alpha_n z) \tag{25}$$

and

$$\lambda_n = -(sin\alpha_n + sh\alpha_n)/(cos\alpha_n + ch\alpha_n) \tag{26}$$

and

$$cos\alpha_n ch\alpha_n + 1 = 0;\ \alpha_n = 1.8751,\ 4.6941,\ 7.8548,\ \ldots \tag{27}$$

$W_n(z)$ can be determined by solving the Euler Bernoulli beam equation in the mode of free beam oscillation at ω_{0n} [37]

$$EI\frac{d^4 W_n(z)}{\partial z^4} - \rho_p A\omega_{0n}^2 W_n(z) = 0 \tag{28}$$

Finally, the beam deflection $u(z)$ and $u'(0)$ can be determined and the load impedance $Z_{L,liquid}$ of the QCM-P operating in water is calculated as

$$Z_{L,liquid} = -\frac{\widehat{\tau}_0}{v_0} = -\frac{N\kappa AG\frac{\partial u}{\partial z}\big|_{z=0}}{j\omega u_0} + j\omega\rho h \tag{29}$$

The governing equations to solve $u'(0)$ and the expansion formula of Eq. (29) in MATLAB are included in the Supplementary Materials.

4. Results and discussion

4.1. QCM-P oscillating in air

The QCM-P devices with micropillar heights ranging from 8 μm to 14.5 μm were operated in air. The complex shear modulus G of the PMMA used in the equivalent circuit model was obtained from literature [32]. The results of frequency shift were compared with those predicted by two-degree-of-freedom model and KLM based QCM-P model as shown in Fig. 5.

As seen in Fig. 5, the frequency shift of the QCM-P device initially decreases linearly with increasing pillar height, which is consistent with the Sauerbrey theory [38]. However, in contrast to a traditional QCM sensor, a sudden "dip and jump" behavior appears at a critical height, H_c, due to the coupled resonance of the piezoelectric substrate and the micropillars. When the micropillar height is less than the critical height, it acts as an inertial loading, resulting in a negative resonant frequency shift. When the height approaches H_c, resonance takes place. If the coupled vibration causes a phase shift less than 90°, the vibration of quartz is damped by the movement of the pillars on its surface, which results in a dip in the negative frequency shift. When the acoustic phase shift is near 90°, micropillar–quartz resonance occurs, leading to a positive frequency shift (normalized to the natural frequency) seen as a jump up in the curve in Fig. 5 (a).

As shown in the Fig. 5, both models predicted the frequency shift of QCM-P accurately. Results show that a low Q-factor was obtained when the micropillar height approaches critical height and resonance occurs.

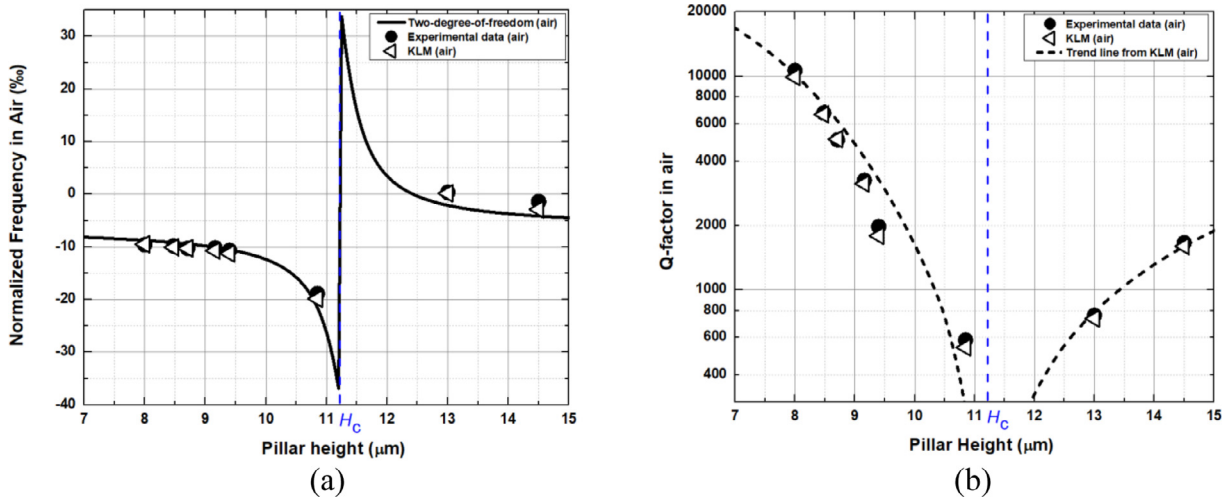

Fig. 5. The comparison of a) frequency shift and b) Q-factor of micropillars operating in air with those predicted by two-degree-of-freedom model (Eq. (2) and KLM based model (Eq. (18)).

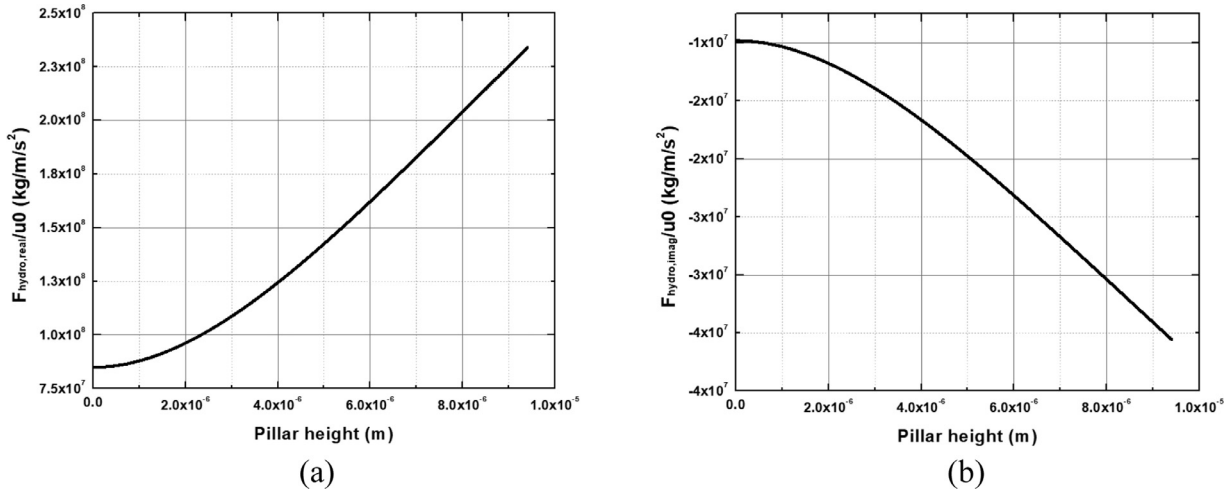

Fig. 6. Hydrodynamic loading on the micropillars (a) real and (b) imaginary components.

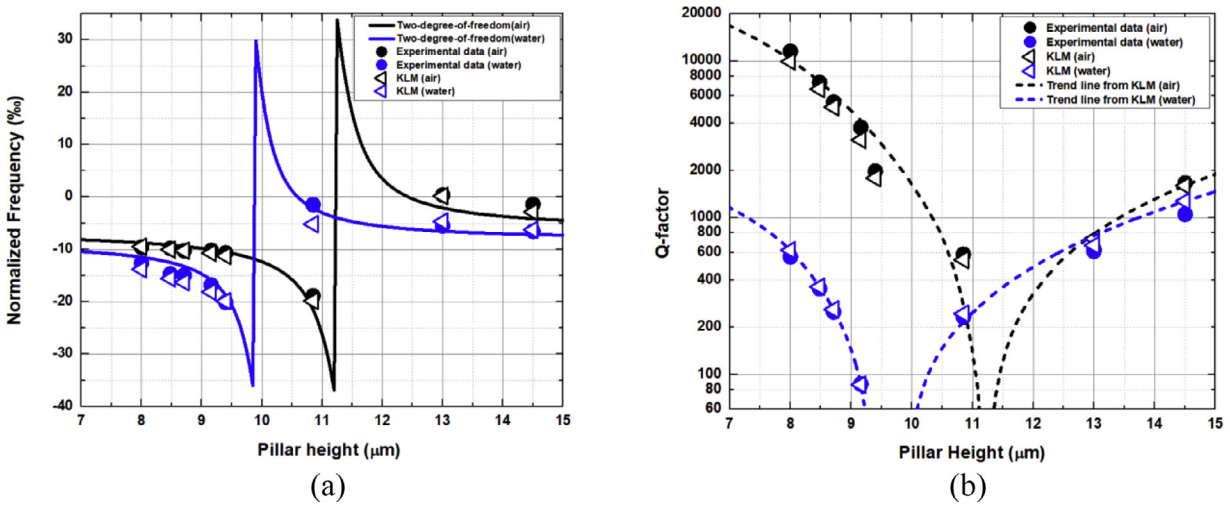

Fig. 7. The comparison of a) frequency shift and b) Q-factor of micropillars operating in air and water with those predicted by two-degree-of-freedom model and KLM based model.

Vibration systems are known to suffer large energy dissipation near resonance [39]. It is believed that the small deviation of the prediction of KLM-based model from the measurement is due to the measurement errors in Young's modulus and complex shear modulus.

4.2. QCM-P oscillating in water

The same QCM-P devices were operated in water and the electrical conductance measurement was performed. The real and imaginary components of the complex hydrodynamic loading were calculated first and the typical results are shown in Fig. 6. The hydrodynamic loading increases with an increase in micropillar height, indicating significant damping to the micropillar vibration.

Fig. 7 presents the predictions from the two-degree-of-freedom model and KLM-based QCM-P model for the micropillar operating in water and air alongside the experimental data.

As seen in Fig. 7, the micropillars exhibit similar trends in frequency shift and Q-factor when operating in water. However, the critical height of the micropillar shifts to a lower value. The reason of the decrease in resonance frequency was that a certain amount of water adhered on the micropillar due to the viscosity effect of water and vibrating together with the micropillar. In the other words, there is a net mass increase of micropillars when operating in the water which induces the decrease in the resonance frequency of the system, described by the real part of hydrodynamic loading. Another observation is that the Q-factors of the micropillars operating in water are much lower than those for micropillars operating in air. This is mainly due to the large energy dissipation caused by the viscous friction of water on the micropillars. It is anticipated that the Q-factor of QCM-P could be lower when the QCM-P devices were used in more viscous body fluids such as blood and saliva.

5. Conclusions

An equivalent-circuit model was developed to predict the Q-factor of QCM-P operating in air and in water with a combined Newton's second law and added mass and damping revision. The model results are in a good agreement with experimental data. The QCM-P exhibits a much higher Q-factor when operating in air in comparison with the low Q-factor (<200) while operating in water. It is believed that the hydrodynamic loading on the micropillars is the main reason for the low Q-factor values or high-energy dissipation. Future research will focus on further improving the equivalent-circuit model by including experimental measurements of shear modulus ($\boldsymbol{G}$) for micropillars and designing other geometries of micropillars.

Declaration of Competing Interest

The authors declare that they have no known competing financial interests or personal relationships that could have appeared to influence the work reported in this paper.

Acknowledgements

The authors thank MicroChem Corp. (Westborough, MA, USA) for providing PMMA material and financial support from National Science Foundation (NSF ECCS 1916374).

Supplementary materials

Supplementary material associated with this article can be found, in the online version, at doi:10.1016/j.snr.2021.100034.

References

[1] KA. Marx, Quartz crystal microbalance: a useful tool for studying thin polymer films and complex biomolecular systems at the solution–surface interface, Biomacromolecules 4 (5) (2003) 1099–1120.
[2] RH. Hall, Biosensor technologies for detecting microbiological foodborne hazards, Microbes Infect. 4 (4) (2002) 425–432.
[3] J. Cai, C. Yao, Ji Xia, J. Wang, M. Chen, J. Huang, K. Chang, C. Liu, H. Pan, W. Fu, Rapid parallelized and quantitative analysis of five pathogenic bacteria by ITS hybridization using QCM biosensor, Sens. Actuators B 155 (2) (2011) 500–504.
[4] L.B. Nie, Y. Yang, S. Li, N.Y. He, Enhanced DNA detection based on the amplification of gold nanoparticles using quartz crystal microbalance, Nanotechnology 18 (30) (2007) 305501.
[5] G. García-Martinez, E.A. Bustabad, H. Perrot, C. Gabrielli, B. Bucur, M. Lazerges, D. Rose, L. Rodriguez-Pardo, J. Fariña, C. Compère, A.A. Vives, Development of a mass sensitive quartz crystal microbalance (QCM)-based DNA biosensor using a 50 MHz electronic oscillator circuit, Sensors (8) (2011) 11.
[6] P. Castro, P. Resa, L. Elvira, Apparent negative mass in QCM sensors due to punctual rigid loading, IOP Conf. Ser. 42 (1) (2012) 012046.
[7] S.J. Martin, V.E. Granstaff, G.C. Frye, Characterization of a Quartz Crystal Microbalance With Simultaneous Mass and Liquid Loading, 63, ETATS-UNIS: American Chemical Society, Washington, DC, 1991.
[8] J.C. Hoogvliet, W.P. van Bennekom, Gold thin-film electrodes: an EQCM study of the influence of chromium and titanium adhesion layers on the response, Electrochim. Acta 47 (4) (2001) 599–611.
[9] J. Su, M. Charmchi, H. Sun, A study of drop-microstructured surface interactions during dropwise condensation with quartz crystal microbalance, Sci. Rep. 6 (2016) 35132.
[10] J. Homola, Surface plasmon resonance sensors for detection of chemical and biological species, Chem. Rev. 108 (2) (2008) 462–493.
[11] C.G. Zhang, C.-.J. Chen, K. Settu, J.-.T. Liu, Angle-scanning surface plasmon resonance system with 3D printed components for biorecognition investigation, Adv. Condens. Matter Phys. 2018 (2018) 5654010.
[12] C.-.S. Lu, O. Lewis, Investigation of film-thickness determination by oscillating quartz resonators with large mass load, J. Appl. Phys. 43 (11) (1972) 4385–4390.
[13] P. Wang, J. Su, W. Dai, G. Cernigliaro, H. Sun, Ultrasensitive quartz crystal microbalance enabled by micropillar structure, Appl. Phys. Lett. 104 (4) (2014) 043504.
[14] P. Wang, J. Su, C-Fu Su, W. Dai, G. Cernigliaro, H. Sun, An ultrasensitive quartz crystal microbalance-micropillars based sensor for humidity detection, J. Appl. Phys. 115 (22) (2014) 224501.
[15] J. Su, H. Esmaeilzadeh, F. Zhang, Q. Yu, G. Cernigliaro, J. Xu, H. Sun, An ultrasensitive micropillar-based quartz crystal microbalance device for real-time measurement of protein immobilization and protein-protein interaction, Biosens. Bioelectron. 99 (2018) 325–331.
[16] S. Butterworth, On electrically-maintained vibrations, Proc. Phys. Soc. Lond. 27 (1) (1914) 410–424.
[17] W.G. Cady, Theory of longitudinal vibrations of viscous rods, Phys. Rev. 19 (1) (1922) 1–6.
[18] K.S. van Dyke, The piezo-electric resonator and its equivalent network, in: Proceedings of the Institute of Radio Engineers, 16, IEEE, 1928, pp. 742–764.
[19] W.H. Chu, Vibration of Fully Submerged Cantilever Plates in Water, South-West Research Institute, 1963 in Technical Report No. 2.
[20] J. Elie Sader, Frequency response of cantilever beams immersed in viscous fluids with applications to the atomic force microscope, J. Appl. Phys. 84 (1) (1998) 64–76.
[21] in C.A. van Eysden, J. Elie Sader, Frequency Response of Cantilever Beams Immersed in Viscous Fluids, in: S.M. Heinrich, F. Josse (Eds.), Resonant MEMS, I.D.O. Brand, 2015. in.
[22] P. Wang, J. Su, L. Gong, M. Shen, M. Ruths, H. Sun, Numerical simulation and experimental study of resonance characteristics of QCM-P devices operating in liquid and their application in biological detection, Sens. Actuators B 220 (2015) 1320–1327.
[23] W.P. Mason, An electromechanical representation of a piezoelectric crystal used as a transducer, Proc. Inst. Radio Eng. 23 (10) (1935) 1252–1263.
[24] W.P. Mason, A dynamic measurement of the elastic, electric and piezoelectric constants of Rochelle salt, Phys. Rev. 55 (8) (1939) 775–789.
[25] A. Ballato, Equivalent circuits for resonators and transducers driven piezoelectrically, Technical Report, 1990 ADA231520.
[26] S. Sherrit, V. Olazabal, J.M. Sansinena, X. Bao, Z. Chang, Y. Bar-Cohen, Use of piezoelectric resonators for the characterization of mechanical properties of polymers, SPIE's 9th Annual International Symposium on Smart Structures and Materials, SPIE, 2002.
[27] R. Krimholtz, D.A. Leedom, G.L. Matthaei, New equivalent circuits for elementary piezoelectric transducers, Electron. Lett. 6 (13) (1970) 398–399.
[28] Y. Jiménez, M. Otero, A. Arnau, Piezoelectric Transducers and Applications, Springer, Berlin, 2004.
[29] T.A. Bigelow, Experimental evaluation of nonlinear indices for ultrasound transducer characterizations, Electrical Engineering, University of Illinois at Urbana-Champaign, Urbana, Illinois, 2001.
[30] R. Lucklum, C. Behling, RW. Cernosek, SJ. Martin, Determination of complex shear modulus with thickness shear mode resonators, J. Phys. D 30 (3) (1997) 346–356.
[31] X. Xie, J. Xie, W. Luo, Z. Wu, Electromechanical coupling and frequency characteristics of a quartz crystal resonator covered with micropillars, J. Vib. Acoust. 141 (4) (2019) 044501-044501-4.
[32] B. Morray, Li Suiqiong, J. Hossenlopp, R. Cernosek, F. Josse, PMMA polymer film characterization using thickness-shear mode (TSM) quartz resonator, in: Proceedings of the 2002 IEEE International Frequency Control Symposium and PDA Exhibition (Cat. No.02CH37234), 2002.
[33] SJ. Martin, HL. Bandey, RW. Cernosek, A.R Hillman, MJ. Brown, Equivalent-circuit model for the thickness-shear mode resonator with a viscoelastic film near film resonance, Anal. Chem. 72 (1) (2000) 141–149.
[34] B. Bhushan, Z. Burton, Adhesion and friction properties of polymers in microfluidic devices, Nanotechnology 16 (2005) 467.
[35] L.D. Landau, E.M. Lifshitz, A.M. Kosevich, J.B. Sykes, L.P. Pitaevskii, W.H. Reid, Theory of Elasticity, Elsevier Science, 1986.
[36] W. Weaver, S.P. Timoshenko, D.H. Young, Vibration Problems in Engineering, Wiley, 1990.
[37] X. Xie, Analysis on the coupled vibrations and frequency shift of a compound system consisting of a quartz crystal plate and surface structures immersed in liquid, Solid Mechanics, Huazhong University of Science & Technology, Wuhan, China, 2017.
[38] G. Sauerbrey, Verwendung von Schwingquarzen zur Wägung dünner Schichten und zur Mikrowägung, Z. Phys. 155 (2) (1959) 206–222.
[39] S.S. Rao, Mechanical Vibrations, Pearson Education, Incorporated, 2017.